Available online at www.sciencedirect.com

ScienceDirect

Geochimica et Cosmochimica Acta 141 (2014) 365–380

Geochimica et Cosmochimica Acta

www.elsevier.com/locate/gca

Modeling the signature of sulfur mass-independent fractionation produced in the Archean atmosphere

Mark W. Claire [a,b,c,*], James F. Kasting [b,d], Shawn D. Domagal-Goldman [b,c,e], Eva E. Stüeken [b,f], Roger Buick [b,f], Victoria S. Meadows [b,g]

[a] Department of Earth and Environmental Sciences, University of St Andrews, Irvine Building, St Andrews, Fife KY16 9AL, UK
[b] NASA Astrobiology Institute – Virtual Planetary Laboratory, University of Washington, Seattle, WA 98195, USA
[c] Blue Marble Space Institute of Science, 1200 Westlake Ave N Suite 1006, Seattle, WA 98109, USA
[d] Department of Geosciences, Pennsylvania State University, 443 Deike Building, University Park, PA 16802, USA
[e] Planetary Environments Laboratory, NASA Goddard Space Flight Center, 8800 Greenbelt Road, Greenbelt, MD 20771, USA
[f] Department of Earth and Space Sciences, University of Washington, 335 Johnson Hall, Seattle, WA 98195, USA
[g] Department of Astronomy, University of Washington, Box 351580, Seattle, WA 98195, USA

Received 18 April 2014; accepted in revised form 28 June 2014; Available online 11 July 2014

Abstract

Minor sulfur isotope anomalies indicate the absence of O_2 from the Archean atmosphere. A rich dataset showing large variations in magnitude and sign of $\Delta^{33}S$ and $\Delta^{36}S$, preserved in both sulfates and sulfides, suggests that further constraints on Archean atmospheric chemistry are possible. We review previous quantitative constraints on atmospheric $\Delta^{33}S$ production, and suggest that a new approach is needed. We added sulfur species containing ^{33}S and ^{34}S to a 1-D photochemical model and describe the numerical methodology needed to ensure accurate prediction of the magnitude and sign of $\Delta^{33}S$ produced by and deposited from the Archean atmosphere. This methodology can test multiple MIF-S formation mechanisms subject to a variety of proposed atmospheric compositions, yielding $\Delta^{33}S$ predictions that can be compared to the rock record. We systematically test SO_2 isotopologue absorption effects in SO_2 photolysis (Danielache et al., 2008), one of the primary proposed mechanisms for $\Delta^{33}S$ formation. We find that differential absorption through the Danielache et al. (2008) cross sections is capable of altering predicted $\Delta^{33}S$ as a function of multiple atmospheric variables, including trace O_2 concentration, total sulfur flux, CO_2 content, and the presence of hydrocarbons, but find a limited role for OCS and H_2S. Under all realistic conditions, the Danielache et al. (2008) cross sections yield $\Delta^{33}S$ predictions at odds with the geologic record, implying that additional pathways for sulfur MIF formation exist and/or the cross sections have significant errors. The methodology presented here will allow for quantitative constraints on the Archean atmosphere beyond the absence of O_2, as soon as additional experimental measurements of MIF-S producing processes become available.

* Corresponding author at: Department of Earth and Environmental Sciences, University of St Andrews, Irvine Building, St Andrews, Fife KY16 9AL, UK. Tel.: +44 (0)1334 463688.
E-mail address: mc229@st-andrews.ac.uk (M.W. Claire).

http://dx.doi.org/10.1016/j.gca.2014.06.032
0016-7037/

1. INTRODUCTION AND BACKGROUND

The presence of mass-independent fractionation in sulfur isotopes (MIF-S or $\Delta^{33/36}S$[1]) is a distinctive feature of sedimentary rocks older than 2.45 Gyr, and constrains paleoatmospheric composition. Both formation and preservation of MIF-S require reducing atmospheric conditions (Farquhar et al., 2000a, 2001; Pavlov and Kasting, 2002; Ono et al., 2003; Zahnle et al., 2006), so the existence of the MIF-S data indicates the near absence of O_2, and the presence of a reducing gas (likely CH_4 and/or H_2). The geologic record preserves time-varying magnitudes and signs of MIF-S in both sulfides and sulfates, along with correlations between $\Delta^{33}S$ and $\Delta^{36}S$. These additional parameters might allow us to infer the concentrations of other gases in the ancient atmosphere, if we can correctly model MIF-S formation, deposition, and preservation (Lyons, 2009; Farquhar et al., 2013; Halevy, 2013). Here, we focus on the methodology to model atmospheric formation and deposition of $\Delta^{33}S$.

The only two mechanisms experimentally shown to produce the coincident large absolute values of $\Delta^{33}S$ and $\Delta^{36}S$ seen in the Archean geologic record involve gas phase SO_2. These are the photolytic destruction of SO_2 (Farquhar et al., 2000a, 2001), an atmospheric reaction $SO_2 + h\nu \rightarrow SO + O$ triggered by absorption of photons ($h\nu$) between 180 and 220 nm (the SO_2 "photolysis band"), and the SO_2 "photoexcitation band" between 250 and 350 nm (Danielache et al., 2012; Whitehill and Ono, 2012; Whitehill et al., 2013), where the absorbed energy is not enough to break the SO_2 bond ($SO_2 + h\nu \rightarrow SO_2^* \rightarrow SO_2$). In the modern atmosphere, O_2 and O_3 absorb UV radiation at wavelengths between 180 and 300 nm, preventing significant tropospheric SO_2 photolysis and MIF-S generation. By contrast, in the absence of O_2/O_3, 180–220 nm photons reach the lower atmosphere, enabling formation of large MIF-S by SO_2 photolysis. More critically, nearly all sulfur input into the modern atmosphere is removed in a single redox state (SO_4^{2-}). The preservation potential of MIF-S is significantly enhanced in reducing atmospheres as these conditions allow sulfur to leave the atmosphere via multiple "exit channels" (sulfate, S_8 aerosol, and/or SO_2), enabling transfer of any generated isotopic heterogeneity to the surface environment (Pavlov and Kasting, 2002; Ono et al., 2003; Halevy et al., 2010; Zerkle et al., 2012). Preservation potential is further enhanced in anoxic oceans, which enable burial of discrete redox phases before isotopic homogenization (Farquhar et al., 2013; Halevy, 2013).

While the presence of large Archean $\Delta^{33}S$ and $\Delta^{36}S$ is widely accepted as indicating a reducing atmosphere (Farquhar et al., 2007; Johnston, 2011), the magnitude and sign of MIF-S is less understood. The Archean data (Fig. 1) show positive and negative $\Delta^{33}S$ values in both sulfides and sulfates. A puzzling asymmetry exists: negative $\Delta^{33}S$ magnitudes rarely extend below −2‰, while positive $\Delta^{33}S$ signals range as high as +12‰. There are multiple possible explanations for the asymmetry, including dilution by biogeochemical processes prior to sedimentation (Halevy et al., 2010), sampling bias, or preservational bias due to scarcity of Archean deep-sea sediments, soils (Maynard et al., 2013) or carbonate-associated sulfate (CAS) data. Preservational bias may be important if the mantle is a long-term reservoir for negative $\Delta^{33}S$ (Farquhar et al., 2002, 2010; Cabral et al., 2013). Alternatively, the asymmetry could result from atmospheric mass balance, whereby a single MIF-S formation mechanism partitions into a dominant reservoir with small magnitude negative $\Delta^{33}S$ and a minor (by mass) exit channel with a correspondingly larger positive $\Delta^{33}S$ signal (Zerkle et al., 2012). This latter interpretation is exemplified by oxygen MIF in the modern atmosphere, which arises during O_3 formation (Thiemens and Heidenreich, 1983). Large positive $\Delta^{17}O$ are seen in quantitatively small exit channels such as nitrate, sulfates, and perchlorates (e.g., Bao and Gu, 2004; Michalski et al., 2004), while the very small negative $\Delta^{17}O$ remains in the much larger reservoir of atmospheric O_2 (Luz et al., 1999).

A widely adopted interpretation of the sign of geologic $\Delta^{33}S$ is that it reflects a single, primary atmospheric source mechanism which partitions into a positive $\Delta^{33}S$ elemental sulfur exit channel and a negative $\Delta^{33}S$ sulfate exit channel (Farquhar et al., 2001; Pavlov and Kasting, 2002; Ono et al., 2003, 2006b, 2009a). This "conventional interpretation" therefore requires that most observed sedimentary sulfides are derived directly from reduced atmospheric species (H_2S or S_8) carrying positive $\Delta^{33}S$, and that most sulfates are derived directly from more oxidized species

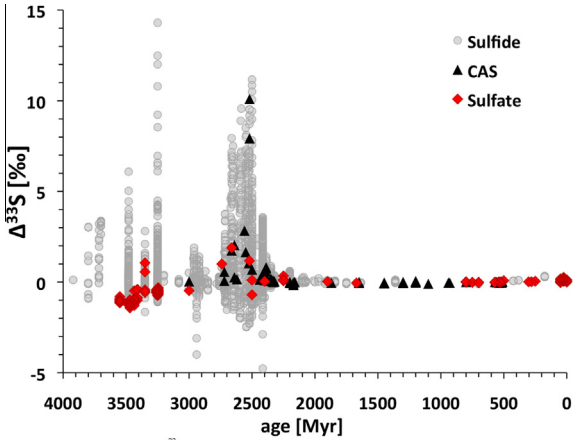

Fig. 1. A compilation of $\Delta^{33}S$ in sedimentary sulfides (grey circles), sulfates (red diamonds), and carbonate associated sulfate (black triangles), updated from the compilation in Stüeken et al. (2012) and references therein, and supplemented with additional data (Fabre et al., 2011; Bontognali et al., 2012; Bühn et al., 2012; Guy et al., 2012; McLoughlin et al., 2012; Philippot et al., 2012; Roerdink et al., 2012, 2013; Grosch and McLoughlin, 2013; Johnson et al., 2013; Kurzweil et al., 2013; Thomazo et al., 2013). Detrital, igneous and hydrothermal sulfides were excluded, as were diamond inclusions and ice-core sulfate data. (For interpretation of the references to color in this figure legend, the reader is referred to the web version of this article.)

[1] $\delta^{3x}S = 1000[(^{3x}S/^{32}S_{model})/(^{3x}S/^{32}S_{standard}) - 1]$, with a standard value of 1 adopted in these calculations. $\Delta^{33}S$ is calculated as $\delta^{33}S - 0.515\ \delta^{34}S$.

(H_2SO_4 or SO_2) carrying negative $\Delta^{33}S$. This interpretation cannot be absolute, as Fig. 1 shows sulfides with negative $\Delta^{33}S$ and sulfates with positive $\Delta^{33}S$, requiring either post-atmospheric transformation in the marine environment (Ono et al., 2009a,b; Shen et al., 2009; Halevy et al., 2010; Farquhar et al., 2013; Halevy, 2013), additional formation reactions with different $\Delta^{33}S$ signatures (Farquhar et al., 2001), or both. The conventional interpretation was rapidly adopted based on early studies that we argue were insufficient to constrain the problem (see Section 4.1); However, multiple recent studies confirm a role for at least one atmospheric production mechanism resulting in positive $\Delta^{33}S$ sulfates and negative $\Delta^{33}S$ sulfides.

1.1. MIF-S production mechanisms

We briefly review proposed MIF-S formation mechanisms. The only non gas-phase mechanisms known to generate MIF-S are the thermochemical reduction of sulfate with organic matter at high temperatures (Watanabe et al., 2009) and liquid phase irradiation of certain organic sulfur compounds (Kopf and Ono, 2012). Both these processes involve a magnetic isotope effect that produces large $\Delta^{33}S$ without corresponding $\Delta^{36}S$, so these mechanisms cannot explain the rock record (Oduro et al., 2011; Kopf and Ono, 2012). Photolysis of CS_2 creates large MIF-S (Zmolek et al., 1999), but calculated CS_2 concentrations remain small even under large biogenic sulfur fluxes (Domagal-Goldman et al., 2011), likely rendering any $\Delta^{33}S$ contributions negligible. H_2S (Farquhar et al., 2000b) and OCS photolysis do not generate large MIF-S (Hattori et al., 2011; Lin et al., 2011), but other potential MIF-S generating reactions have been suggested, including (but not limited to) SO photolysis (Ono et al., 2003), $S + S_2 \rightarrow S_3$ (Du et al., 2011), and SO_3 photolysis (Pavlov et al., 2005). These latter pathways are hypothetical and considered unlikely (Lyons, 2009) but are worthy of future research (Domagal-Goldman et al., 2012), given the multiple formation pathways suggested by the data (Farquhar et al., 2001; Lyons, 2009; Ono et al., 2009a, 2013; Masterson et al., 2011; Whitehill and Ono, 2012; Whitehill et al., 2013). Given that thirteen years of laboratory investigations have consistently demonstrated large magnitude $\Delta^{33}S$ and $\Delta^{36}S$ signals stemming from SO_2 photolysis, this process is probably the most important in explaining the Archean record. However, at least one additional formation pathway, likely involving SO_2 photo(de)excitation, is almost certainly also involved.

The polyatomic SO_2 molecule has both rotational and vibrational quantum states, creating a complex absorption spectrum that varies over sub-nanometer wavelength scales (Okabe, 1978). Differential absorption of photons by isotopologue-dependent absorption cross-sections could lead to MIF-S in both the photolysis and photoexcitation bands. MIF-S could also (or additionally) arise from changes in isotopologue-specific reaction rates that occur subsequent to the initial absorption, but prior to the disassociation or relaxation back to the SO_2 ground state. If this latter case holds, the details of the initial SO_2 photon absorption process may be less important to MIF-S generation than is currently assumed. The precise mechanism by which MIF-S arises in each of these SO_2 bands remains an area of active research.

In our Archean model atmospheres, SO_2 concentrations generally peak below 15 km (e.g., Fig. 2a), so MIF-S can be affected if any high-altitude species absorb 180–220 or 250–320 nm photons before they can reach SO_2 molecules in the lower atmosphere. This phenomenon is broadly defined as 'shielding' of SO_2 by those gases or particles (Ueno et al., 2009). "Self-shielding" is a special case of shielding which occurs if there is sufficient SO_2 such that $^{32}SO_2$ absorbs all photons of a certain wavelength by a given height in the atmosphere. This condition of "optically thick SO_2" precludes further $^{32}SO_2$ photolysis at that wavelength lower in the column, but enables photons that interact with $^{33/34/36}SO_2$ to propagate lower in the atmosphere, generating a characteristic MIF-S due to preferential photolysis of $^{33/34/36}SO_2$ but not $^{32}SO_2$ (Lyons, 2007).

Laboratory experiments are identifying important mechanisms involved in MIF-S production, but direct application to the rock record requires caution, as experimental setups often use gas concentrations and illumination conditions which are not likely to occur in an actual atmosphere. One such experiment that has been over-interpreted is the "193 nm array" of Farquhar et al. (2001), in which a narrow band laser was used to photolyze SO_2. We have full confidence in the experimental result, but show in Section 4.1.1 that the partitioning into positive $\Delta^{33}S$ sulfide and negative $\Delta^{33}S$ sulfates is strongly dependent on the laser used, and therefore not directly relevant to the Archean atmosphere. Experiments using broadband light sources are more broadly applicable, although it remains important to acknowledge that the experimental data are relevant to conditions in the photocells, which might not be representative of the natural atmosphere. Broadband light sources also produce negative $\Delta^{33}S$ in sulfates (Masterson et al., 2011; Whitehill and Ono, 2012; Ono et al., 2013), although the high partial pressures of SO_2 in the photocells enables SO_2 self-shielding behavior (Lyons, 2007) producing $\Delta^{33}S/\delta^{34}S$ and $\Delta^{33}S/\Delta^{36}S$ patterns not observed in the Archean record (Ono et al., 2013). Experiments are approaching SO_2 partial pressures relevant to the natural atmosphere (Masterson et al., 2011; Whitehill and Ono, 2012; Whitehill et al., 2013), and are confirming that SO_2 photolysis generally produces negative $\Delta^{33}S$ sulfates with strong dependence on pressure, temperature, and wavelength. Much experimental and theoretical work remains to be done, but it does appear clear that (a) interaction of SO_2 with both 180–220 nm and 250–320 nm photons generates MIF-S, and (b) reducing conditions are needed to preserve that signal. A primary aim of this paper is to describe the minimum theoretical framework needed to translate experimental results into accurate modeling predictions of MIF-S produced in the atmosphere.

1.2. Previous modeling of Archean MIF-S

Pavlov and Kasting (2002) performed the first photochemical modeling study of sulfur isotopes in the early

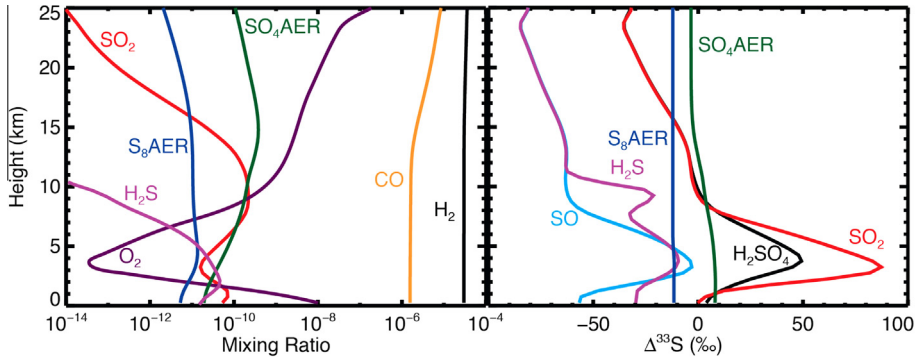

Fig. 2. The "standard model" atmosphere. (a) Mixing ratios of atmospheric gases and aerosols (SO_4AER and S_8AER are sulfate and elemental sulfur particles, respectively). (b) Computed $\Delta^{33}S$ versus height in the atmosphere.

atmosphere. This study yielded multiple insights including: (a) the demonstration that MIF-S (once produced) rapidly partitions between all other atmospheric sulfur species; (b) the importance of multiple "exit channels" in the delivery of MIF-S to the surface; and (c) the identification of 10^{-5} PAL O_2 as the upper limit for the Archean atmosphere. The upper limit for Archean O_2 was significant in that it was a much stronger constraint than could be drawn from other geochemical proxies (e.g., Holland, 1984; Catling and Claire, 2005). The constraint originates from the inability to construct a model atmosphere with 10^{-5} PAL O_2 that could maintain an elemental sulfur (S_8) exit channel, while atmospheres with 10^{-15} PAL O_2 could. Despite this ten order of magnitude gap in their modeled O_2 concentrations, the constraint has held up and remains a strong upper limit on Archean O_2 concentrations. The existing laboratory data did not allow Pavlov and Kasting (2002) to make quantitative predictions of $\Delta^{33}S$; rather, they assumed fractionation factors for SO_2 photolysis, and showed they would propagate through the atmospheric system.

Studies following on from Pavlov and Kasting (2002) adopted the deposition rate of S_8 aerosols (Ono et al., 2003; Zahnle et al., 2006) or SO_2 photolysis rates (Domagal-Goldman et al., 2008) as a proxy for MIF-S, with only implicit links to the magnitude of MIF-S. The modeled parameter space of reducing atmospheres was expanded, and three major influences on S_8 deposition were identified: total sulfur, O_2, and CH_4 (Ono et al., 2003; Zahnle et al., 2006). The Mesoarchean minimum in $\Delta^{33}S$ was briefly interpreted as reflecting oxygenation (Ohmoto et al., 2006; Ono et al., 2006a), but consideration of $\Delta^{33}S/\Delta^{36}S$ slopes revealed that all Archean sulfides result from mass-independent processes (Farquhar et al., 2007; Johnston, 2011). Formation of an organic haze at high CH_4:CO_2 concentrations was also shown to decrease SO_2 photolysis rates in a 1-D photochemical model (Domagal-Goldman et al., 2008), suggesting that shielding by organic haze might have caused the diminution of $\Delta^{33}S$ magnitudes in the Mesoarchean.

The measurement of photolysis band absorption cross sections for $^{32}SO_2$, $^{33}SO_2$, and $^{34}SO_2$ by Danielache et al. (2008) (henceforth DA08) enabled the first quantitative $\Delta^{33}S$ predictions for the Archean atmosphere (Ueno et al., 2009; Halevy et al., 2010). However, neither of these studies used a 1-D photochemical model. Using the DA08 cross sections, Ueno et al. (2009) noted that (integrated) SO_2 photolysis between 180 and 200 nm produces sulfate with negative $\Delta^{33}S$, while SO_2 photolysis between 200 and 220 nm produces sulfate with positive $\Delta^{33}S$. Invoking the conventional MIF-S interpretation, they argued that atmospheric opacity between 200 and 220 nm must therefore have been greater than between 180 and 200 nm. Only O_3 and OCS have absorption cross sections that increase with wavelength between 180 and 220 nm (Ueno et al., 2009). As large MIF-S indicates the absence of O_3 from the Archean atmosphere, Ueno et al. (2009) suggested that positive $\Delta^{33}S$ in sulfides was induced by large quantities of atmospheric OCS preferentially absorbing 200–220 nm photons, shielding SO_2 from photolysis. Using a one-box model, they concluded that 5 ppm of OCS in an atmosphere with more CO than CO_2 was needed to explain the Archean $\Delta^{33}S$ record.

We are unconvinced that such an atmospheric state could have existed. Archean OCS concentrations above 10 ppb are unlikely due to rapid OCS photolysis (Domagal-Goldman et al., 2011; Zerkle et al., 2012, Fig. A6). Furthermore, atmospheric CO:CO_2 ratios higher than 1 are also unlikely after the evolution of life (Kharecha et al., 2005), as CO is readily consumed by a wide range of microbes. Perhaps more importantly, we also question the methodology used to derive these conclusions, and argue that a one-box model does not resolve the altitude-dependent complexities in chemical composition and redox necessary to accurately simulate dry and wet deposition from the Archean atmosphere. For example, Ueno et al. (2009) argued that any Archean atmosphere with more CO_2 than CO is too oxidizing to produce MIF-S, a conclusion that is contradicted by Fig. 2 and by other studies of Archean atmospheric structure and redox state (Pavlov and Kasting, 2002; Ono et al., 2003; Zahnle et al., 2006; Domagal-Goldman et al., 2008; Zerkle et al., 2012; Kurzweil et al., 2013). The lack of vertical resolution in their model may have inflated the role for oxidation by CO_2 photolysis, which is important in the oxidized upper stratosphere, but does not occur in the lower atmosphere where CO_2 is optically thick. That said, the key insight of Ueno et al. (2009) remains valid: atmospheric opacity to

SO_2 photolysis between 180 and 220 nm is vital for understanding the MIF-S record.

Halevy et al. (2010) also utilized the DA08 cross sections to predict Archean $\Delta^{33}S$. Their study used a simple vertical atmospheric structure, and assumed that H_2S with zero MIF-S mixes (and dilutes) MIF-S produced by one (parameterized) disproportionation reaction: $2SO_2 + h\nu \rightarrow SO + SO_3$. The SO was assumed to form S_8 aerosol, while SO_3 became sulfate aerosol, and these products were immediately removed from the model atmosphere. In more complex models of the Archean atmosphere, the dominant atmospheric SO sink is the pressure-dependent recombination to SO_2 ($SO + O + M \rightarrow SO_2 + M$, where M is a third species such as N_2), and this and approximately 80 other reactions (Pavlov and Kasting, 2002; Domagal-Goldman et al., 2011, this study) must be accounted for to accurately predict gaseous sulfur concentrations. Halevy et al. (2010) predicted negative $\Delta^{33}S$ sulfates and positive $\Delta^{33}S$ sulfides in all atmospheric cases, in apparent disagreement with the Ueno et al. (2009) study that required 5 ppm OCS in a 1% CO atmosphere to accomplish this. However, the Halevy et al. (2010) results were obtained by assuming the atmosphere was completely opaque to UV radiation between 200 and 220 nm because of the presence of some unspecified gas. Our numerical predictions agree with Halevy et al. (2010) only in the unphysical case where we integrate SO_2 photolysis between 180 and 200 nm but not between 200 and 220 nm (see Appendix II), a scenario for which no atmospheric absorber is known. We agree with the Halevy et al. (2010) key insight that post-depositional processes will affect the magnitude of $\Delta^{33}S$ stored in the rock record, but we question their quantitative $\Delta^{33}S$ predictions and the conclusions drawn from them. We contend that a 1-D photochemical model is required to make accurate quantitative predictions of Archean redox structure and MIF-S production.

2. MODEL DESCRIPTION

Our 1-D photochemical model incorporates 74 gas-phase species undergoing 392 photochemical reactions (83 and 424, respectively, for the biogenic sulfur runs in Fig. A6). The model (Zahnle et al., 2006; Domagal-Goldman et al., 2011; Zerkle et al., 2012) includes vertical transport by eddy and molecular diffusion, rainout, lightning, particle condensation, and diffusion-limited hydrogen escape. The altitude grid runs from the surface to 100 km in 0.5 km increments, with a fixed tropopause height of 11 km. Radiative transfer was computed using the δ 2-stream methodology (Toon et al., 1989) incorporating both Rayleigh scattering by gases and Mie scattering by particles (Yung, 1976). Photolysis rates were diurnally-averaged and assumed a 50° solar zenith angle. Model equations were integrated using a variable time-step reverse-Euler method suitable for stiff systems, which relaxes to the steady-state (Newton's method) solution when model time steps are large. We ensure convergence by integrating until the model is able to take 10 billion year time steps without changing any species concentration or flux by more than a factor of 10^{-12}. In practice, well behaved models subject to slight perturbations converge toward new steady state solutions between 100 and 10,000 model years, but the added computation improves the redox balance. To assess reliability, we check that all model simulations balance the internal atmospheric redox budget to better than one part per billion, and verify that the lower boundary fluxes needed to create the given numerical solution are broadly consistent with plausible fluxes from Archean biology and/or volcanic activity.

Fig. 2a shows gas concentrations from a "standard model" constructed to be representative of late Archean atmospheric composition after the evolution of oxygenic photosynthesis but before the Great Oxidation Event (Zerkle et al., 2012). The standard atmosphere was computed with a 2.5 Ga solar flux (Claire et al., 2012), with a volcanic sulfur flux of 3.85×10^9 molecules cm^{-2} s^{-1} ($\sim$1 Tmol yr^{-1}) at an H_2S:SO_2 ratio of 1:10 and a volcanic H_2 flux of 1×10^{10} molecules cm^{-2} s^{-1} ($\sim$3 Tmol yr^{-1}). The volcanic inputs were distributed vertically throughout the troposphere in a lognormal fashion. CO_2 concentrations were fixed at 1% at all heights, and N_2 provided a total atmospheric pressure of 1 bar. Further boundary conditions imposed include fixed ground-level mixing ratios of 100 ppm and 10 ppb for CH_4 and O_2, respectively. To maintain these mixing ratios in steady-state with all other processes, the model computed fluxes of 3.6×10^{11} molecules cm^{-2} s^{-1} and 6.2×10^{11} molecules cm^{-2} s^{-1}, respectively, which are broadly consistent with predictions of Archean biospheric fluxes of CH_4 and O_2 after the evolution of oxygenic photosynthesis (Kasting et al., 2001; Pavlov and Kasting, 2002; Kharecha et al., 2005; Canfield et al., 2006; Zahnle et al., 2006). A reducing atmosphere is maintained by volcanic fluxes for H_2 and H_2S slightly enhanced from the modern (Case 'V2' of Zahnle et al., 2006) and by a CH_4:O_2 flux ratio $>$ 1:2 (Catling et al., 2007; Kurzweil et al., 2013). Although organic haze might have been present in the Mesoarchean (Pavlov et al., 2001; Domagal-Goldman et al., 2008; Kurzweil et al., 2013) and for short durations in the Neoarchean (Zerkle et al., 2012), we assume a "clear skies" condition for our standard atmosphere, which is maintained by our choice of CH_4:CO_2 ratio of 0.01 (Trainer et al., 2006). The relatively simple particle formation scheme has not been substantially updated since the work of Pavlov and Kasting (2002). As with previous studies, our S_8 production peaks in the lower troposphere (not shown), but minor production leads to trace S_8 aerosol concentrations in the lower stratosphere. Our predicted concentrations (and therefore $\Delta^{33}S$ predictions) may be affected by over-estimations of polysulfur vapor pressures (Lyons, 2008) and/or our boundary conditions that require a finite fall velocity at height. Updating the sulfur and organic aerosols schemes represents an important avenue for future research.

Our results are sensitive to our assumption of a "late Archean" biosphere, specifically, the inclusion of an O_2 flux from oxygenic photosynthesis. In the standard model, the O_2 lifetime against loss at the ground is 9 h. Given that the primary source of O_2 requires sunlight, the Archean atmosphere might have exhibited diurnal, spatial, and/or seasonal changes in local oxygen concentrations. In a 1-D globally

averaged model however, fluxes must be considered as a distributed planetary average. Therefore, our standard model should not be considered valid only over an "oxygen plume" in a localized highly productive region, but rather as a representative average. By analogy, our inclusion of volcanic H_2S, SO_2, CO_2, and H_2 fluxes does not restrict our validity to near a volcanic plume – rather, we are attempting to model the quiescent background atmosphere subject to the net yearly flux of these gases. Unlike O_2, these volcanic gases have long photochemical lifetimes, so our model predictions involving a tropospheric source of free O_2 are not likely to be valid extremely far from a source region. This implies that the Archean atmosphere could produce heterogeneous $\Delta^{33}S$ signals depending on the degree of interaction with tropospheric O_2, and that our standard model predictions are most representative of a coastal shelf or shallow sea environment with high primary productivity. These near shore environments tend to be preserved preferentially in the sedimentary rock record compared to non-marine or deep-marine settings.

We enhance our well-established 1-D photochemical model to calculate the $\Delta^{33}S$ generated by a given atmospheric state subject to various MIF-S formation mechanisms. First, we integrate $^{32}SO_2$ – along with the other atmospheric species – to steady state. At that steady-state solution, $^{33}SO_2$ and $^{34}SO_2$ are independently computed in isotopic equilibrium with $^{32}SO_2$ and other $^{33/34}S$ bearing species following established methods (Pavlov and Kasting, 2002). Unlike the Pavlov and Kasting (2002) study, however, arbitrary fractionation factors are not assumed; rather, all fractionation arises from the differential absorption/emission of UV radiation by SO_2 isotopologues, as modulated by the presence of other gases in the model atmosphere. The magnitude and sign of $\Delta^{33}S$ is therefore a model prediction, not a tuning parameter. To ensure accurate MIF-S computations, we enhanced our photolysis and radiative transfer schemes to use a variable wavelength grid, which is easily modifiable depending on the MIF-S formation mechanism under study. For most of the work presented here, we use a 0.05 nm wavelength grid between 180 and 220 nm, resolving the vibronic bands of SO_2 to the accuracy of the DA08 $^{32}SO_2$, $^{33}SO_2$, and $^{34}SO_2$ cross sections, with a 0.01 nm grid for the Schumann–Runge bands of O_2 (Zerkle et al., 2012), and the standard "JPL 1983 grid" otherwise. This methodology computes only mass-independent contributions to the sulfur isotope budget, so while computed $\Delta^{33}S$ represents a prediction to be compared to the rock record, the absolute $\delta^{33}S$ and $\delta^{34}S$ values are not. Addition of the reactions affecting the mass-dependent chemistry of atmospheric sulfur species is certainly feasible within this methodology, but was beyond the scope needed for this work. Further discussion and validation of our isotopic computations are presented in Appendix I. We wish to stress that the methodology developed here is easily extendable to new isotopologue-specific cross sections and/or reaction rate data as they become available, as well as for testing alternate mechanisms. Furthermore, the methodology is extendable to make computations of $\Delta^{36}S$ when appropriate data become available.

3. RESULTS

3.1. SO_2 self-shielding

We first investigate if SO_2 self-shielding could be important in the quiescent Archean atmosphere. The peak SO_2 mixing ratio of ~0.5 ppb occurs in the lower stratosphere near the tropopause (Fig. 2a), with photolytic loss depressing the mixing ratio below. A secondary SO_2 peak occurs lower in the troposphere due to the volcanic input. The overall atmospheric response to ~1 Tmol SO_2 yr^{-1} leads to a total column density of 1×10^{15} SO_2 molecules cm^{-2} with a corresponding SO_2 optical depth of 0.03. This Archean volcanic flux estimate is uncertain, and Zahnle et al. (2006) suggest it could have been 3 times higher. Fig. 3 shows results from model runs with SO_2 fluxes ranging from modern to 40 times modern. Even at the extreme SO_2 flux case, the SO_2 absorption optical depth remains below 0.1, far below the ~1 needed for self-shielding. In the Archean, like today, SO_2 self-shielding would only occur in volcanic plumes, which can increase the SO_2 column density by orders of magnitude in the days to weeks following a large eruption. Although potentially relevant for specific volcanic-rich horizons (Thomazo et al., 2009; Philippot et al., 2012), it seems unlikely that SO_2 self-shielding in the occasional volcanic plume would significantly affect the bulk fractionation integrated into the Archean geologic record. Given that our standard model produces substantial $\Delta^{33}S$ (Fig. 2b), prodigious amounts of $\Delta^{33}S$ would have to emanate from occasional plumes to quantitatively overprint the $\Delta^{33}S$ from the quiescent background atmosphere.

3.2. Investigating the Danielache et al. (2008) cross sections

Next, we simulated thousands of plausible, self-consistent, late Archean atmospheric compositions using our updated 1-D photochemical model to predict $\Delta^{33}S$ resulting from the DA08 180–220 nm photolysis cross sections, with results shown in Figs. 2, 6, 7 and Appendix III-a. Fig. 2b shows the computed $\Delta^{33}S$ values from our representative late Archean atmosphere. Using DA08, our standard

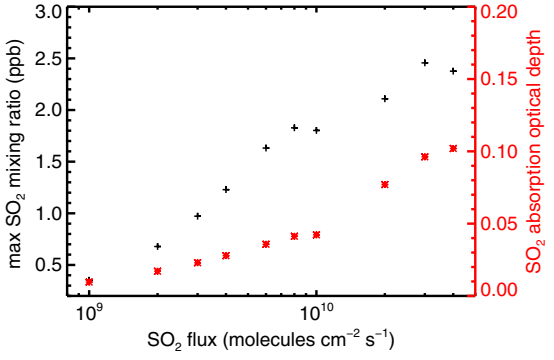

Fig. 3. Peak SO_2 mixing ratio (black plus symbols, left axis) and absorption optical depth (red star symbols, right axis) as a function of SO_2 flux. (For interpretation of the references to color in this figure legend, the reader is referred to the web version of this article.)

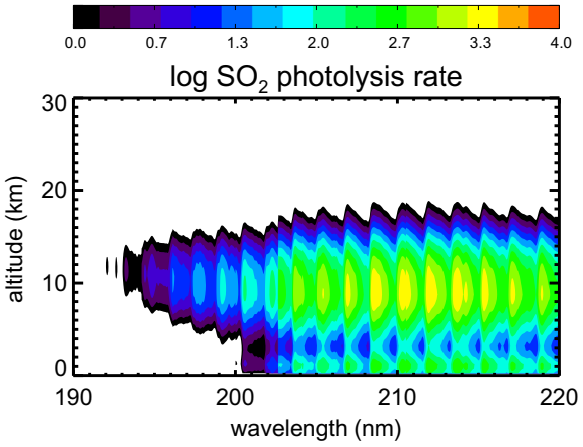

Fig. 4. Contour of the wavelength and height dependences of the SO_2 photolysis rate ($cm^3\ s^{-1}$) in our standard model atmosphere.

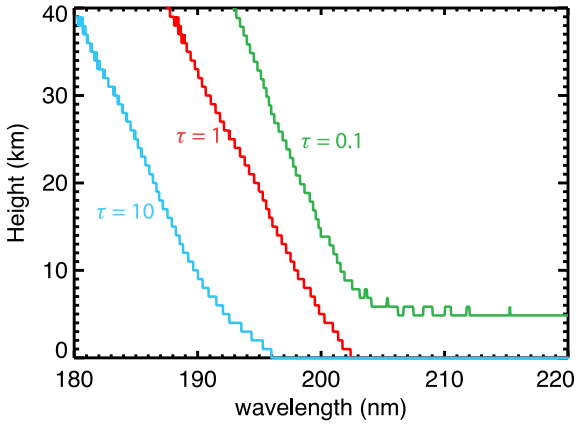

Fig. 5. Depth of penetration of atmospheric photons in our standard model. Each trace shows the height at which photons starting from the top of the atmosphere reach the indicated optical depth, τ.

atmosphere produces sulfate with positive $\Delta^{33}S$ and S_8 with negative $\Delta^{33}S$, inconsistent with the conventional interpretation of MIF-S. Compared to models without a photosynthetic O_2 source (Pavlov and Kasting, 2002; Ono et al., 2003), SO_2 is also a quantitatively significant exit channel, with positive $\Delta^{33}S$ in SO_2 delivered to the surface by a combination of wet and dry deposition. Given its high solubility and $\Delta^{33}S$ variability (Fig. 2b), SO_2 in particular requires integration over a vertically resolved troposphere to accurately predict the $\Delta^{33}S$ delivered to the surface. While the ~2/3 of SO_2 that leaves via dry deposition with $\Delta^{33}S$ of −0.2‰ reflects mixing with zero MIF-S volcanic SO_2, the remaining 1/3 of SO_2 dissolved in rain takes on a net $\Delta^{33}S$ of ~+15‰, leading to a total predicted $\Delta^{33}S$ of ~+5‰ for SO_2 in our standard model (Table 1). The short lifetime of O_2, compounded with its affect on the SO_2 exit channel, further indicates the potential for spatial and temporal differences in Neoarchean $\Delta^{33}S$.

The prediction of positive $\Delta^{33}S$ sulfate using DA08 extends to the entire parameter space explored in this study. Independent of cross section used, all model atmospheres reveal SO_2 photolysis rates increasing with wavelength (Fig. 4), so the bulk of the $\Delta^{33}S$ signal is generated from SO_2 photolysis reactions between 200 and 220 nm. This trend results from 3 factors: (1) the CO_2 absorption band weakens by 5 orders of magnitude between 180 and 206 nm, which allows for increasing penetration of solar photons to the lower atmosphere; (2) there is a ~50-fold increase in the number of solar photons between 180 and 220 nm; and (3) while many gases absorb at wavelengths less than 200 nm, atmospheric gases other than O_3 have generally weak absorption from 200 to 220 nm (Ueno et al., 2009). Fig. 4 demonstrates that SO_2 photolysis does not occur at wavelengths less than 192 nm in the standard model, and that most SO_2 photolysis occurs between 205 and 215 nm. The $\Delta^{33}S$ variability in SO_2 seen in Fig. 2b is directly related, as different wavelengths of light interact with SO_2 at various heights (Fig. 4), imparting unique $\Delta^{33}S$ signatures. Fig. 5 shows that photons with wavelengths less than ~195 nm do not reach to the troposphere. 202 nm and longer wavelength photons reach the ground, but with some tropospheric attenuation through 220 nm, consistent with the SO_2 photolysis rates shown in Fig. 4. Barring the presence of organic haze (Zerkle et al., 2012), realistic atmospheric compositions with significant opacity at wavelengths longer than 200 nm do not appear feasible for reducing early Earth atmospheres (Fig. 5). When organic hazes do form, the resulting atmospheres (Figs. 7 and A7) also produce positive $\Delta^{33}S$ sulfate. Therefore, the model prediction of positive $\Delta^{33}S$ in atmospherically-produced sulfate is robust to the extent that the DA08 $^{3X}SO_2$ cross sections are accurate and no other MIF-S generating process significantly influences the Archean record.

Figs. 6, 7 and A6–A8 show photochemical model runs with boundary conditions differing from the standard model. The top panels show ground-level mixing ratios and fluxes of important species, while the bottom panels show DA08 $\Delta^{33}S$ predicted in SO_2, SO_4 and S_8 delivered to the surface, along with their corresponding exit channel fractions. Each panel shows extracted data products from ~100 model atmospheres run at identical boundary conditions, excepting only the independent variable on the x-axis. Any bulk uncertainties inherent in our standard model are therefore maintained throughout each suite of model runs. This manner of analysis effectively normalizes any error in the standard model, affording confidence that trends result from the given change in the independent variable.

We first explore model sensitivity to changing fluxes of volcanic and biogenic sulfur gases. Our model predicts minimal changes in $\Delta^{33}S$ resulting from varying the SO_2 to H_2S ratio in the volcanic gas flux, but reveals marked $\Delta^{33}S$ changes with total sulfur flux (Figs. 6 and A6). This lack of correlation between the ratio of input sulfur gases and steady-state concentrations is contrary to the findings of Halevy et al. (2010), but is consistent with other models (Ono et al., 2003; Zahnle et al., 2006) that compute atmospheric chemistry with quantitatively significant fluxes of additional redox gases. Changes to the reducing volcanic fluxes on the order of 1×10^{10} molecules $cm^{-2}\ s^{-1}$ do not have a major influence on the instantaneous atmospheric

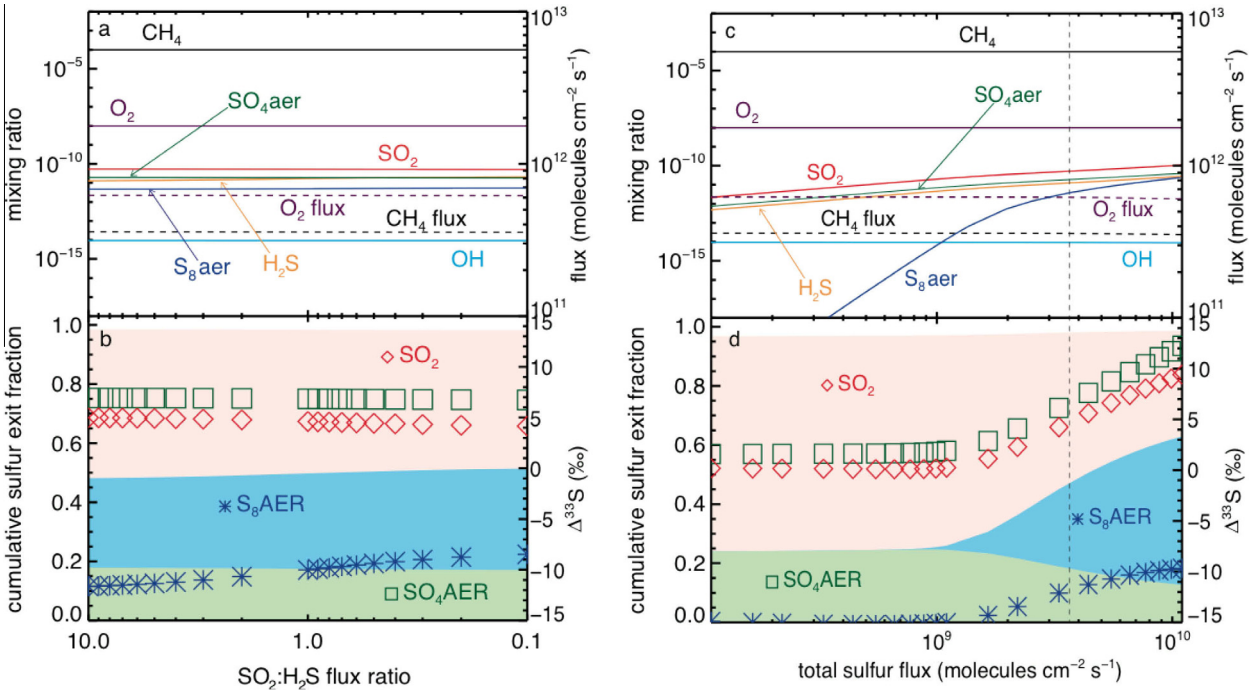

Fig. 6. The response of our model to (a and b) changing SO_2:H_2S in volcanic gas, and (c and d) total sulfur flux, both shown on the horizontal axis. The standard model is the left most atmosphere at 10:1 SO_2:H_2S, and is represented by a dashed line on (c) and (d) (and subsequent panels). Top panel – surface volume mixing ratios (solid lines) map to left axis, while fluxes (dashed lines) map to right axis. Bottom panel – Sulfur exit channel fractions are shown as shaded regions (sulfate – light green, S_8 – light blue, SO_2 – light red), mapped to left axis. Net $\Delta^{33}S$ delivered to the surface are shown as symbols (sulfate – dark green squares, S_8 – dark blue stars, SO_2 – dark red diamonds), mapped to the right axis. (For interpretation of the references to color in this figure legend, the reader is referred to the web version of this article.)

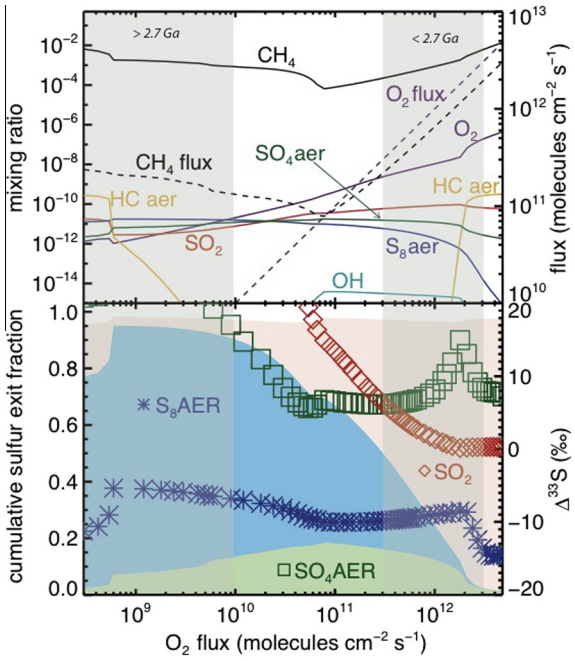

Fig. 7. The response of our model to changing the methane and oxygen fluxes in the manner described by Kurzweil et al. (2013). The grey shaded regions labeled ">2.7 Ga" and "<2.7 Ga" reflect their preferred atmospheric conditions before and after the evolution of oxygenic photosynthesis. Colors and symbols as in Fig. 6.

redox state when the CH_4 fluxes are ~50 times greater. Due to their photochemical reactivity, these inorganic sulfurous gases quickly interconvert and relax to concentrations dictated by the overall atmospheric redox state, which in our model is driven by more inert (and therefore plentiful) gases such as H_2 and CH_4. As a result, the input ratio of SO_2 to H_2S (Fig. 6a and b) has little bearing on their steady-state concentrations, as our model is free to make minor adjustments to the larger redox terms in order to balance the fixed mixing ratio boundary conditions on O_2 and CH_4. While a changing SO_2:H_2S ratio could affect the global redox balance (Kasting, 2013) with potential long-term effects for the evolution of the ocean–atmosphere system (Kump and Barley, 2007; Holland, 2009), the direct chemical effect on our modeled reducing atmospheres is negligible. By contrast, increasing the total amount of S gases (in whatever fraction or form) enhances S_8 formation rates, with subsequent changes in $\Delta^{33}S$ (Fig. 6c and d). This behavior is further supported by calculations in which biogenic sulfur gases are varied (see Appendix III-a).

Intermittent hydrocarbon haze has recently been proposed during the Archean (Zerkle et al., 2012; Kurzweil et al., 2013). While this interpretation stems from variations in the $\Delta^{33}S/\Delta^{36}S$ slope beyond the scope of this study, we can investigate how haze affects $\Delta^{33}S$ computed using DA08. Kurzweil et al. (2013) presented photochemical models run at varying fluxes of CH_4 and O_2, and simulated the evolution of oxygenic photosynthesis. Fig. 7a reproduces their Fig. 5a and contains simulations of hazy and

Table 1
Atmospheric exit fluxes (molecules cm^{-2} s^{-1}) and $\Delta^{33}S$ (‰) in the dominant sulfur exit channels in the standard model, and the standard model modified to include the 250–320 nm photoexcitation band (Danielache et al., 2012). In the latter case, discussed in Appendix III-b, we utilize a wavelength grid with 0.05 nm resolution from 180 to 320 nm (0.01 nm in the Schuman–Runge bands). The $^{3x}SO_2$ cross sections used were a hybrid of Danielache et al. (2008) from 180 to 250 nm and Danielache et al. (2012) from 250 to 320 nm. In each model, HS and H_2S made up the remainder of the mass balance, each at ~0.2% of the total output with $\Delta^{33}S$ of −17‰ and −30‰, respectively.

Species	Dry deposition flux	$\Delta^{33}S$ in dry deposition	Rainout flux	Integrated $\Delta^{33}S$ in rain	Total $\Delta^{33}S$ at surface	Exit channel fraction
Standard model (integration of 180–220 nm photolysis band using DA08)						
HSO	1.54E+07	−30.46	7.97E+06	−27.51	−29.45	0.006
H_2SO_4	1.81E+07	3.86	1.63E+07	12.31	7.86	0.009
SO_2	1.37E+09	−0.23	5.55E+08	17.85	4.98	0.50
SO_4AER	5.53E+06	8.04	6.81E+08	6.91	6.92	0.18
S_8AER	1.19E+07	−11.58	1.15E+09	−11.65	−11.65	0.30
Standard model with 250–320 nm photoexcitation band included						
HSO	1.56E+07	−29.38	8.01E+06	−26.48	−28.40	0.006
H_2SO_4	1.82E+07	3.70	1.63E+07	11.86	7.54	0.009
SO_2	1.37E+09	−0.25	5.51E+08	17.15	4.73	0.50
SO_4AER	5.52E+06	7.76	6.81E+08	6.69	6.70	0.18
S_8AER	1.20E+07	−11.01	1.16E+09	−11.08	−11.08	0.30

clear atmospheres both prior to a large O_2 flux (left side) and with significant biogenic fluxes of O_2 and CH_4 (right side). Interestingly, the two hazy states have distinctive dominant reactions, exit channel fractions and $\Delta^{33}S$, so we postulate that organic hazes before and after the evolution of oxygenic photosynthesis might yield unique sulfur isotope signatures. The high O_2/hazy regime (Fig. 7b, right side) has $\Delta^{33}S$ approaching 0‰ as the SO_2 exit channel dominates, while the high O_2/clear-sky regime features relatively large and positive $\Delta^{33}S$ magnitudes, similar to the standard model. The low O_2/hazy regime (Fig. 7b, left side) provides an exception to our general result that large $\Delta^{33}S$ magnitudes correlate with smaller exit channel fractions. The clear sky regions in both low and high O_2 fluxes (i.e., within the grey shaded regions of Fig. 7 where the hydrocarbon aerosol (HCAER) has mixing ratio less than 10^{-12}) illustrates the range of potential variability in global conditions on post oxygenic-photosynthesis world, encompassing regions near and far from a O_2 source region and their differences in SO_2 deposition.

There is scope for further updating the modeling of Archean organic haze. Since publication of Domagal-Goldman et al. (2008), the importance of "fractal" particle scattering of UV/visible photons has been suggested (Wolf and Toon, 2010). The results shown in Figs. 7 and A7 were run using Mie scattering. Zerkle et al. (2012) presented coupled $\Delta^{33}S/\Delta^{36}S/\delta^{13}C_{org}$ data indicating transient Neoarchean haze, and also provided the first Archean atmospheric models incorporating fractal haze particles. Both UV and visible optical depths change dramatically from the clear-skies cases shown in Figs. 2–6, and also differ between the fractal and Mie scattering cases (Wolf and Toon, 2010; Zerkle et al., 2012). These changes in haze optical depth lead to changes in the dominant sulfur reaction rates and exit channels (Zerkle et al., 2012; Kurzweil et al., 2013), which leads to changes in the predicted $\Delta^{33}S$ (Figs. 7 and A7). None of these recent models include accurate coupling of climatic effects of haze (e.g., Haqq-Misra et al., 2008), nor higher-order hydrocarbon reactions needed to accurately model Titan's atmosphere (e.g., Hebrard et al., 2013), both of which lie beyond the scope of this study. Here, we simply wish to highlight that organic haze due to elevated CH_4 concentrations is one of multiple atmospheric vectors that could have modulated the $\Delta^{33}S$ record.

4. DISCUSSION

Using the DA08 cross sections, our model predicts positive $\Delta^{33}S$ in sulfates and negative $\Delta^{33}S$ in S_8 which is contrary to the conventional interpretation of the Archean record, in which negative $\Delta^{33}S$ is assumed to arise from sulfate and positive $\Delta^{33}S$ from sulfides or S_8. We consider the following explanations:

(1) The DA08 SO_2 cross sections used to generate the $\Delta^{33}S$ predications are inaccurate.
(2) SO_2 photolysis is not the only MIF-S generating reaction that contributes to the Archean geologic record.
(3) Sampling or preservational bias exists in the Archean sedimentary sulfur isotope record.
(4) The conventional interpretation of $\Delta^{33}S$ sign requires revision.

Explanation 1 has been suggested (Lyons, 2009; Blackie et al., 2011) based on rotational complexity not recorded in the DA08 data. This higher resolution fine structure is likely necessary to compute the $\Delta^{33}S$ contribution by SO_2 self-shielding (Lyons, 2007, 2009; Ono et al., 2013), which certainly occurs in the high SO_2 optical depths of laboratory experiments (Farquhar et al., 2001; Masterson et al., 2011; Whitehill and Ono, 2012; Ono et al., 2013). In the natural atmosphere, SO_2 self-shielding is only relevant in dense volcanic plumes (Lyons, 2009; Hattori et al., 2013; Ono et al., 2013) where $^{32}SO_2$ temporarily becomes optically thick, but this is unlikely to quantitatively swamp

the significant $\Delta^{33}S$ produced continuously by the quiescent background atmosphere (Figs. 2, 6 and 7) with optically thin SO_2 (Figs. 3–5). Therefore, the inability of these cross sections to account for SO_2 self-shielding is not enough to discard them. More problematically, the overall accuracy of these cross sections have been called into question (Whitehill and Ono, 2012). Furthermore, the DA08 cross-sections were measured at SO_2 partial pressures greater than natural abundance (0.2–9.3 mbar), and so could contain pressure-dependent effects not relevant to the natural atmosphere. We share major concerns over the data quality of the DA08 cross sections,[2] although we note that Monte-Carlo calculations incorporating the reported measurement errors (Fig. A4) support the primary result of positive $\Delta^{33}S$ in sulfates, leaving a systematic offset in the $^{33}SO_2$ spectra as the most likely mechanism for error (Whitehill and Ono, 2012; Ono et al., 2013). Additional measurements of all four SO_2 isotopologue cross sections are needed to resolve these doubts.

Explanation 2 is almost certainly true as well, and we highlight the often-overlooked conclusion of Farquhar et al. (2001) that multiple formation pathways were needed to explain their experimental SO_2 photolysis data. The SO_2 photoexcitation band generates MIF-S (Danielache et al., 2012; Hattori et al., 2013; Whitehill et al., 2013), and has recently been implicated in MIF-S creation in modern stratospheric volcanic plumes (Hattori et al., 2013). These modern MIF-S signals are measured directly in sulfate aerosols in plumes or in ice cores (Savarino et al., 2003; Baroni et al., 2007, 2008), on samples that are not likely to be preserved in the permanent geologic record of our era. Given that reducing conditions are more conducive to preserving MIF-S signatures, the SO_2 photoexcitation band represents an important target for Archean research. Incorporation of the SO_2 photoexcitation cross sections (Danielache et al., 2012) alone has little effect on our standard model (see Appendix III-b for further discussion), but incorporation of the newly demonstrated effects of photo de-excitation (Whitehill et al., 2013) is beyond the scope of this study.

The further possibility exists that the Archean sedimentary S isotope record is substantially biased (Explanation 3), either by sampling or preservation. Archean sulfates and CAS are severely undersampled relative to sulfides, so a more balanced record might show a dominance of positive sulfates. There are few Archean records of sulfur isotopes from subductable sulfide or sulfate in or on oceanic crust (Farquhar et al., 2010), so there may be a mantle sink of opposite sign that is not well represented in the crustal record (Farquhar et al., 2002, 2010; Cabral et al., 2013). Lastly, it is possible that poorly preserved non-marine Archean environments, particularly soils, hosted a crustal reservoir of sulfur species of opposite sign to their marine equivalents (Maynard et al., 2013).

[2] The cross sections we use are not those published as 2007jd009695-ds01.txt by DA08. We utilize a file named 'data-non-systematic-errors-corrections.txt' provided to us by Sebastian Danielache in 2011. Use of these cross sections alters the magnitudes of our predicted $\Delta^{33}S$ signal, but does not affect the conclusions regarding the sign.

4.1. The genesis of the conventional interpretation of MIF-S

Accepting our modeling results at face value would indicate that the Archean atmosphere produced sulfates with positive $\Delta^{33}S$ and sulfides with negative $\Delta^{33}S$, in contrast to the conventional interpretation of MIF-S (Explanation 4), so a few words on the origin of the interpretation are warranted. This interpretation (Ono et al., 2003) arose based on two early papers which showed negative $\Delta^{33}S$ in 3.4 billion year old sulfate materials (Farquhar et al., 2000a) and follow-up laboratory experiments at 193 nm which created sulfates with negative $\Delta^{33}S$ (Farquhar et al., 2001). While more recent data and experiments provide additional evidence for the conventional interpretation, we note that these two early pieces were not sufficient for widespread adoption of the interpretation.

4.1.1. The 193 nm array

Fig. 8a shows the SO_2 photolysis fractionation factors between 192 and 194 nm (Danielache et al., 2008). These factors represent the instantaneous $\Delta^{33}S$ in SO resulting from the (non-self-shielded) SO_2 photolysis reaction at the given wavelength, resulting only from photon absorption by amplitude variations in the SO_2 isotopologue absorption cross-sections. These cross-sections reveal $\Delta^{33}S$ fractionation factors that oscillate between $-400‰$ to $+800‰$ over wavelength ranges of ~0.01 nm. Therefore, predicting the net fractionation from SO_2 photolysis requires integration over the entire wavelength range of interest. The (grey) shaded region is the approximate emission spectrum of the Farquhar et al. (2001) ArF laser, which was centered at 193 nm with a 1 nm Gaussian dispersion. Fig. 8b shows the product of the fractionation factor and the laser, while the legend shows this value integrated over wavelength. The net prediction for photolysis with this 193 nm laser is positive $\Delta^{33}S$ in SO, and therefore negative $\Delta^{33}S$ in the residual SO_2 and sulfates that form from it, confirming the results of the 2001 laboratory experiments. While we have full confidence in the experimental results of Farquhar et al. (2001), we join Lyons (2009) in questioning their direct applicability to the Archean rock record, given the sensitivity of our calculations to the UV light source used. For example, a similar integration (Fig. 8c and d) for a hypothetical laser centered at 192.5 nm predicts positive $\Delta^{33}S$ in sulfates and negative $\Delta^{33}S$ in sulfides. Thus, it would appear that Farquhar et al. (2001) serendipitously produced negative $\Delta^{33}S$ sulfates. A corollary is that 193 nm photolysis experiments should not be used to directly interpret the sign of MIF-S in the rock record.

4.1.2. Early Archean barites

The 3.48 Ga Dresser Formation contains sulfate with $\Delta^{33}S$ averaging near $-1‰$ (Farquhar et al., 2000a; Philippot et al., 2007; Ueno et al., 2008; Shen et al., 2009). Fig. 9 shows barite crystals from the Dresser Formation, found within stromatolitic structures (Buick, 1985). However, it is not clear that these barites formed directly

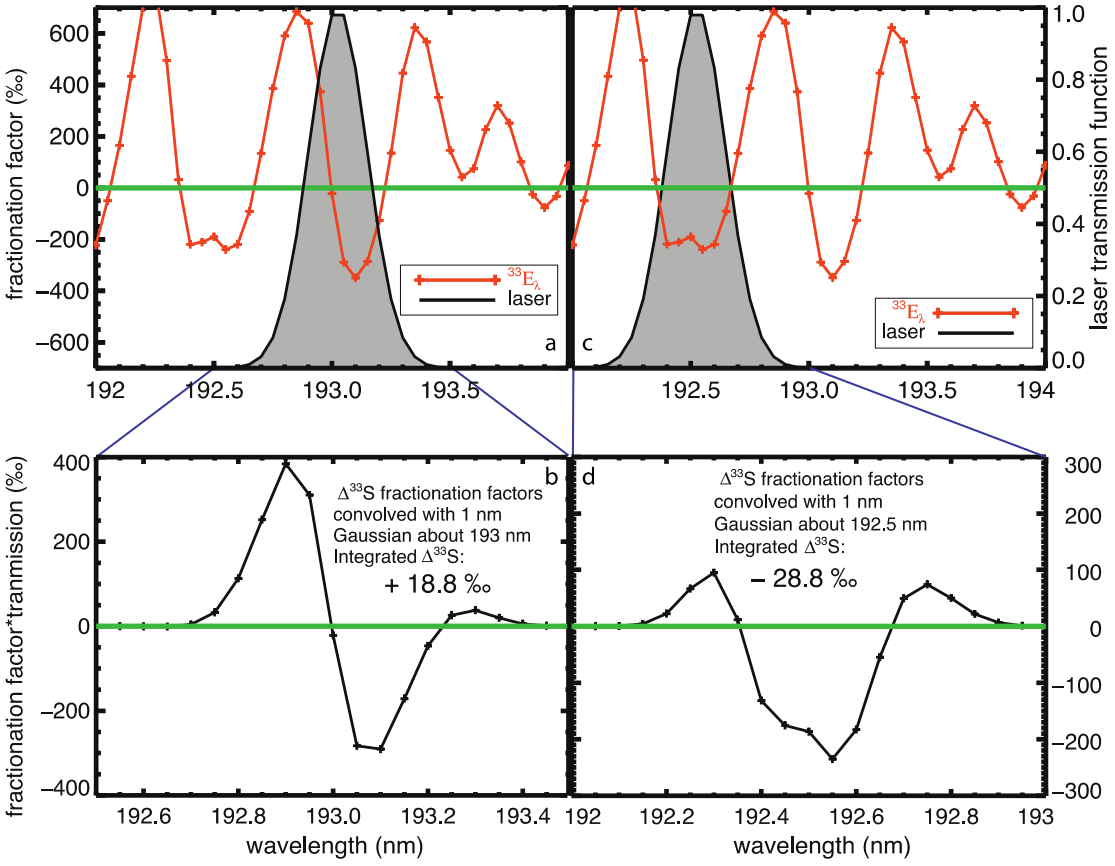

Fig. 8. (a and c) Process-independent SO_2 photolysis fractionation factors ($^{33}E_\lambda$) (Danielache et al., 2008; Ueno et al., 2009) (left axis, orange curves) and a laser transmission functions (right axis, grey shaded region) of Farquhar et al. (2001). (b and d) Multiplication of the fractionation factor with the transmittance, with resultant area under the curve (the net fractionation imparted to SO) shown on the legend.

from atmospherically derived sulfate. It has been argued that the sulfate in these barites was formed by microbial oxidation of reduced S (H_2S or S_8), either via anoxygenic photosynthesis or via chemotrophic S oxidation with O_2 or nitrate (Shen and Buick, 2004; Olson, 2006). The barite is in some places intimately interbedded with stromatolitic structures that appear to have been accreted by phototropic microbes as indicated by their laminae thickening over flexure crests, further supporting a biotic sulfate source (Buick et al., 1981, Fig. 9). Sulfide oxidation leading to gypsum deposition in anoxygenic photosynthetic microbial mats has recently described for thrombolites in a hypersaline lagoon (Petrash et al., 2012), providing a potential modern analog for this model of the Dresser Formation.

While measurements on other Archean sulfates not closely associated with stromatolites also yield predominantly negative $\Delta^{33}S$ (Bao et al., 2007; Ueno et al., 2008; Roerdink et al., 2012), this evidence does not rule out the possibility that these sulfates could have sourced from sulfur species other than atmospheric sulfate (Olson, 2006). The conventional interpretation of the sulfates, carrying a negative $\Delta^{33}S$, would require formation directly from a pool of atmospherically-derived sulfate, perhaps in an evaporatic setting. While we find the biological precipitation scenario more likely, this is not the key argument we wish to make. Here, we simply seek to highlight the uncertainty of the ultimate sulfur source, which limits credibility for these barites to underpin the conventional interpretation of MIF-S.

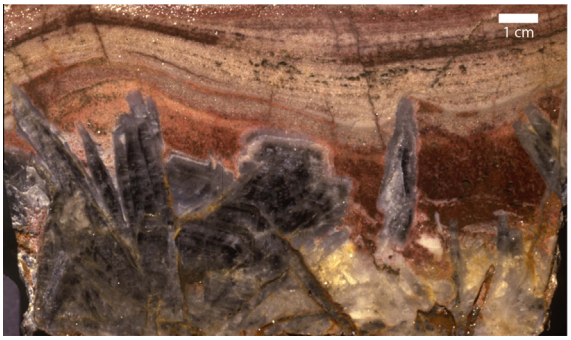

Fig. 9. Dresser Formation Barite crystals (photo credit – Roger Buick).

4.2. A discussion on the conventional interpretation

While the conventional interpretation was widely adopted based on two early pieces of evidence we find

unconvincing, there is a large dataset of measurements and experiments that support negative $\Delta^{33}S$ sulfates so the interpretation is not easily discarded. As previously discussed, our $\Delta^{33}S$ predictions are correct only if: (1) the cross-sections we used are accurate and (2) non-optically thick SO_2 photolysis is the primary processes contributing to Archean $\Delta^{33}S$, both of which have difficulties but are certainly within the realm of possibility. A third explanation was that the Archean sulfur MIF record was incompletely sampled. For the 4th alternative (that the conventional interpretation of the $\Delta^{33}S$ record requires revision) to be feasible, we find that the 3rd option (that the geological record is biased either by sampling or preservation) must obtain to some degree, as follows.

If our modeled sign inversion for sulfate and sulfide $\Delta^{33}S$ is correct (i.e., we invoke Explanation 4), then some corollary evidence should be present in the isotopic record. One might expect a preponderance of positive $\Delta^{33}S$ Archean sulfates but this not the case, with the record being overwhelmingly dominated by samples with $\Delta^{33}S = <0‰$ (Fig. 1). It is important to note that these negative $\Delta^{33}S$ sulfates predominantly occur prior to 3.2 Ga, and so may not bear at all on Meso or Neoarchean atmospheric composition. It could then be argued that much of the positive $\Delta^{33}S$ Neoarchean sulfate was converted to sulfides by mass-dependent fractionation processes such as microbial sulfate reduction, especially if sulfate concentrations were generally low in the Archean ocean such that it was a limiting nutrient for this metabolism. If this were the case, a spread of $\delta^{34}S$ values extending leftwards from the Archean array on a $\Delta^{33}S/\delta^{34}S$ diagram should be evident, but again that is not the case. Instead, the bulk of sulfide data plot leftward of the cluster of negative $\Delta^{33}S$ sulfate values as if mass-dependently fractionated from them (e.g., Ono et al., 2003). Given this, to get the isotopically homogeneous cluster of sulfate $\Delta^{33}S$ and $\delta^{34}S$ values by oxidation of this heterogeneously negative sulfide population in the absence of a significant positive $\delta^{34}S$ fractionation upon sulfide oxidation, a similarly heterogeneous set of $\Delta^{33}S/\Delta^{36}S$ ratios might be expected in the sulfate population, but again this seems not to occur, with well-correlated (bulk) trends towards negative $\Delta^{33}S$ and positive $\Delta^{36}S$ such that $\Delta^{33}S \approx -\Delta^{36}S$ (Ueno et al., 2008; Shen et al., 2009; Roerdink et al., 2012). Indeed, sedimentary pyrites from the same rocks show heterogeneous deviations from this $\Delta^{33}S/\Delta^{36}S$ trend most consistent with derivation from the sulfate by microbial reduction, rather than the converse (sulfates derived from sulfides by microbial oxidation). Thus, the extant isotopic record does suggest an additional level of support for the conventional interpretation.

Given the suspect foundations of the conventional $\Delta^{33}S$ interpretation, and the associated uncertainties with experiments and the fundamental processes that create MIF-S, we can at least speculate about Explanation 4 in conjunction with our model results. If DA08 are sufficient and our model results are accurate predictions of the Archean atmosphere, the large spike in positive $\Delta^{33}S$ seen in Neoarchean sulfides would require a formation process deriving from atmospheric sulfate. Reasonable variations in the atmospheric composition considered here (in total volcanic or biogenic sulfur, organic haze, or increasing trace O_2) could lead to increasingly positive $\Delta^{33}S$ sulfates, while simultaneously producing reduced sulfur species with lower magnitude negative $\Delta^{33}S$. The Neoarchean data could then be explained by transformation of positive $\Delta^{33}S$ sulfate by microbial sulfate reduction, with negative $\Delta^{33}S$ sulfides deriving from elemental sulfur/polysulfide acting as an alternate pyrite precursor in sediments (Farquhar et al., 2013). The high total sulfur (Figs. 6c, d and A6) and the low O_2 atmospheres (left side of Fig. 7) may best reflect this scenario. This interpretation is supported by carbonate-associated sulfates measured between 2.7 and 2.5 Ga, which show exclusively positive $\Delta^{33}S$ (Fig. 1), although many of these measurements might contain contamination from pyrite (Domagal-Goldman et al., 2008). Increased (but rapidly recycled) Neoarchean sulfate concentrations are further supported by data indicating contemporaneous sulfide oxidation on land (Stüeken et al., 2012), the evolution of oxygenic photosynthesis (Kurzweil et al., 2013), partial oxygenation of surface oceans (e.g., Kendall et al., 2010; Farquhar et al., 2011; Zerkle et al., 2012), and microbial sulfate reduction metabolism (Shen and Buick, 2004; Ueno et al., 2008; Shen et al., 2009; Roerdink et al., 2012; Farquhar et al., 2013).

Invoking Explanation 4 would therefore require that most sedimentary sulfides stem from microbial sulfate reduction in conjunction with a missing global reservoir of sulfur. These conditions, while certainly plausible, are not without difficulties given the extensive Archean sulfur isotope dataset, and are hard to justify given uncertainties in the experimental data and MIF-S formation processes. In particular, a strong validation of the DA08 cross-sections seems necessary before serious consideration of an argument to re-interpret the sulfur isotope record. As a result, we favor a combination of Explanations 1 and 2 for explaining the sign of $\Delta^{33}S$ predicted using the DA08 cross sections. Given that multiple atmospheric process can modulate $\Delta^{33}S$ (a general result) and that specific predictions stemming from the DA08 cross sections may be revised, we refrain from making additional constraints on the composition of the Archean atmosphere at this time.

5. CONCLUSIONS

The source mechanism(s) for MIF-S in the Archean atmosphere is not yet fully understood. We have argued that vertical heterogeneity in composition and redox state renders box models insufficient for accurate predictions of $\Delta^{33}S$, leading us to question the quantitative conclusions of Ueno et al. (2009) and Halevy et al. (2010). While calling for more experiments to unravel the mechanisms modulating MIF-S, we caution against the direct applicability of experimental results to the Archean atmosphere, in particular SO_2 self-shielding and 193 nm laser experiments. We describe an easily adaptable methodology needed to predict $\Delta^{33}S$ in atmospheric exit channels, and show that multiple atmospheric compositions could have modulated the $\Delta^{33}S$ signal, implying that attempts to use the $\Delta^{33}S$

record alone to constrain Archean gas compositions (beyond O_2) are likely premature. While the isotopologue cross sections used in this study may affect details of our quantitative predictions, we have confirmed that $\Delta^{33}S$ magnitudes are generally inversely correlated with exit channel mass balance (Zerkle et al., 2012; Kurzweil et al., 2013) implying that the carrier of negative $\Delta^{33}S$ was likely the larger exit channel in the Archean.

We specifically tested $\Delta^{33}S$ signatures using the SO_2 photolysis cross sections of Danielache et al. (2008) and the SO_2 photoexcitation cross sections of Danielache et al. (2012), which universally predict positive $\Delta^{33}S$ in sulfates and negative $\Delta^{33}S$ in sulfides. If these cross sections are accurate and no other process contributes MIF-S, the Neoarchean rise in positive $\Delta^{33}S_{sulfide}$ fractionation could be explained by increasing O_2, total sulfur, or clearing of an organic haze, but requires that Neoarchean pyrites obtained most of their S from microbial sulfate reduction or SO_2. The feasibility of this claim could be tested by comprehensive models tracking the atmospheric source to sedimentation (Lyons, 2009; Halevy, 2013) and may be falsifiable by careful evaluation of pyrite formation pathways (Ono et al., 2009a; Farquhar et al., 2013) and the existing geologic record. A more likely explanation is that the DA08 cross sections have errors and that multiple processes contribute to the Archean sulfur MIF record.

Future prospects for constraining atmospheric MIF-S are bright, as new photolysis cross sections appear to be on the horizon (Danielache et al., 2012) and newly discovered photo de-excitation effects may contribute to the Archean record (Whitehill et al., 2013). In particular, precise measurements of $^{36}SO_2$ cross sections will enable us to exploit the extra degree of freedom in the $\Delta^{33}S/\Delta^{36}S$ data, perhaps resolving some of the causative multiplicity inherent in $\Delta^{33}S$ predictions alone. As our methodology is easily adaptable to new experimental data, quantitative atmospheric constraints beyond the simple presence or absence of O_2 are likely obtainable from the Archean sulfur isotope record in the near future.

ACKNOWLEDGEMENTS

MC would like to thank Sebastian Danielache for providing cross-section data, and Aubrey Zerkle and James Farquhar for helpful conversations. Boz Wing and Shuhei Ono are thanked for careful reviews that improved this manuscript. The NASA Astrobiology Institute (NAI) is acknowledged for funding a NASA postdoctoral program fellowship to the lead author and all authors acknowledge the NAI funding for the Virtual Planetary Laboratory, supported by NASA under cooperative agreement NNH05ZDA001C.

APPENDIX A. SUPPLEMENTARY DATA

Supplementary data associated with this article can be found, in the online version, at http://dx.doi.org/10.1016/j.gca.2014.06.032.

REFERENCES

Bao H. M. and Gu B. H. (2004) Natural perchlorate has a unique oxygen isotope signature. *Environ. Sci. Technol.* **38**, 5073–5077.

Bao H., Rumble, III, D. and Lowe D. R. (2007) The five stable isotope compositions of Fig Tree barites: implications on sulfur cycle in ca. 3.2 Ga oceans. *Geochim. Cosmochim. Acta* **71**, 4868–4879.

Baroni M., Thiemens M. H., Delmas R. J. and Savarino J. (2007) Mass-independent sulfur isotopic compositions in stratospheric volcanic eruptions. *Science* **315**, 84–87.

Baroni M., Savarino J., Cole-Dai J., Rai V. K. and Thiemens M. H. (2008) Anomalous sulfur isotope compositions of volcanic sulfate over the last millennium in Antarctic ice cores. *J. Geophys. Res. Atmos.*, 113.

Blackie D., Blackwell-Whitehead R., Stark G., Pickering J. C., Smith P. L., Rufus J. and Thorne A. P. (2011) High-resolution photoabsorption cross-section measurements of SO_2 at 198 K from 213 to 325 nm. *J. Geophys. Res. Planets*, 116.

Bontognali T. R. R., Sessions A. L., Allwood A. C., Fischer W. W., Grotzinger J. P., Summons R. E. and Eiler J. M. (2012) Sulfur isotopes of organic matter preserved in 3.45-billion-year-old stromatolites reveal microbial metabolism. *Proc. Natl. Acad. Sci. USA* **109**, 15146–15151.

Bühn B., Santos R. V., Dardenne M. A. and de Oliveira C. G. (2012) Mass-dependent and mass-independent sulfur isotope fractionation (delta S-34 and delta S-33) from Brazilian Archean and Proterozoic sulfide deposits by laser ablation multi-collector ICP-MS. *Chem. Geol.* **312**, 163–176.

Buick R. (1985) *Life and Conditions in the Early Archaean: Evidence from 3500 m.y. Old Shallow-Water Sediments in the Warrawoona Group, North Pole, Western Australia*. University of Western Australia, p. 353.

Buick R., Dunlop J. S. R. and Groves D. I. (1981) Stromatolite recognition in ancient rocks: an appraisal of irregularly laminated structures in an early Archean chert-barite unit from North Pole, Western Australia. *Alcheringa* **5**, 161–181.

Cabral R. A., Jackson M. G., Rose-Koga E. F., Koga K. T., Whitehouse M. J., Antonelli M. A., Farquhar J., Day J. M. D. and Hauri E. H. (2013) Anomalous sulphur isotopes in plume lavas reveal deep mantle storage of Archaean crust. *Nature* **496**, 490–493.

Canfield D. E., Rosing M. T. and Bjerrum C. (2006) Early anaerobic metabolisms. *Philos. Trans. R. Soc. Lond. B* **361**, 1819–1834.

Catling D. C. and Claire M. W. (2005) How Earth's atmosphere evolved to an oxic state: a status report. *Earth Planet. Sci. Lett.* **237**, 1–20.

Catling D. C., Claire M. W. and Zahnle K. J. (2007) Anaerobic methanotrophy and the rise of atmospheric oxygen. *Philos. Trans. R. Soc. Lond. A* **365**, 1867–1888.

Claire M. W., Sheets J., Cohen M., Ribas I., Meadows V. S. and Catling D. C. (2012) The evolution of solar flux from 0.1 nm to 160 microns: quantitative estimates for planetary studies. *Astrophys. J.*, 757.

Danielache S. O., Eskebjerg C., Johnson M. S., Ueno Y. and Yoshida N. (2008) High-precision spectroscopy of (32)S, (33)S, and (34)S sulfur dioxide: ultraviolet absorption cross sections and isotope effects. *J. Geophys. Res. Atmos.*, 113.

Danielache S. O., Hattori S., Johnson M. S., Ueno Y., Nanbu S. and Yoshida N. (2012) Photoabsorption cross-section measurements of S-32, S-33, S-34, and S-36 sulfur dioxide for the B1-X1A1 absorption band. *J. Geophys. Res. Atmos.*, 117.

Domagal-Goldman S., Johnston D., Farquhar J. and Kasting J. F. (2008) Organic haze, glaciations, and multiple sulfur isotopes in the Mid-Archean Era. *Earth Planet. Sci. Lett.* **269**, 29–40.

Domagal-Goldman S., Meadows V. S., Claire M. W. and Kasting J. F. (2011) Using biogenic sulfur gases as remotely detectable biosignatures on anoxic planets. *Astrobiology* **11**, 1–23.

Domagal-Goldman S., Poirier B. and Wing B. (2012). Mass-Independent Fractionation of Sulfur Isotopes: Carriers and Sources. NASA Workshop Report <http://is.gd/s_mif>, Alexandria, VA, p. 36.

Du S. Y., Germann T. C., Francisco J. S., Peterson K. A., Yu H. G. and Lyons J. R. (2011) The kinetics study of the $S + S_2 \rightarrow S_3$ reaction by the chaperone mechanism. *J. Chem. Phys.*, 134.

Fabre S., Nedelec A., Poitrasson F., Strauss H., Thomazo C. and Nogueira A. (2011) Iron and sulphur isotopes from the Carajas mining province (Para, Brazil): implications for the oxidation of the ocean and the atmosphere across the Archaean–Proterozoic transition. *Chem. Geol.* **289**, 124–139.

Farquhar J., Bao H. and Thiemans M. (2000a) Atmospheric influence of Earth's earliest sulfur cycle. *Science* **289**, 756–758.

Farquhar J., Savarino J., Jackson T. L. and Thiemans M. H. (2000b) Evidence of atmospheric sulfur in the martian regolith from sulphur isotopes in meteorites. *Nature* **404**, 50–52.

Farquhar J., Savarino J., Airieau S. and Thiemens M. H. (2001) Observation of wavelength-sensitive mass-independent sulfur isotope effects during SO_2 photolysis: application to the early atmosphere. *J. Geophys. Res.* **106**, 1–11.

Farquhar J., Wing B. A., McKeegan K. D., Harris J. W., Cartigny P. and Thiemens M. H. (2002) Mass-independent sulfur of inclusions in diamond and sulfur recycling on early Earth. *Science* **298**, 2369–2372.

Farquhar J., Peters M., Johnston D. T., Strauss H., Masterson A., Wiechert U. and Kaufman A. J. (2007) Isotopic evidence for Mesoarchaean anoxia and changing atmospheric sulphur chemistry. *Nature* **449**, 706–709.

Farquhar J., Wu N., Canfield D. E. and Oduro H. (2010) Connections between sulfur cycle evolution, sulfur isotopes, sediments, and base metal sulfide deposits. *Econ. Geol.* **105**, 509–533.

Farquhar J., Zerkle A. L. and Bekker A. (2011) Geological constraints on the origin of oxygenic photosynthesis. *Photosynth. Res.* **107**, 11–36.

Farquhar J., Cliff J., Zerkle A. L., Kamyshny A., Poulton S. W., Claire M., Adams D. and Harms B. (2013) Pathways for Neoarchean pyrite formation constrained by mass-independent sulfur isotopes. *Proc. Natl. Acad. Sci. USA* **110**, 17638–17643.

Grosch E. G. and McLoughlin N. (2013) Paleoarchean sulfur cycle and biogeochemical surface conditions on the early Earth, Barberton, South Africa. *Earth Planet. Sci. Lett.* **377**, 142–154.

Guy B. M., Ono S., Gutzmer J., Kaufman A. J., Lin Y., Fogel M. L. and Beukes N. J. (2012) A multiple sulfur and organic carbon isotope record from non-conglomeratic sedimentary rocks of the Mesoarchean Witwatersrand Supergroup, South Africa. *Precambrian Res.* **216**, 208–231.

Halevy I. (2013) Production, preservation, and biological processing of mass-independent sulfur isotope fractionation in the Archean surface environment. *Proc. Natl. Acad. Sci. USA*.

Halevy I., Johnston D. T. and Schrag D. P. (2010) Explaining the structure of the Archean mass-independent sulfur isotope record. *Science* **329**, 204–207.

Haqq-Misra J. D., Domagal-Goldman S. D., Kasting P. J. and Kasting J. F. (2008) A revised, hazy methane greenhouse for the Archean Earth. *Astrobiology* **8**, 1–11.

Hattori S., Danielache S. O., Johnson M. S., Schmidt J. A., Kjaergaard H. G., Toyoda S., Ueno Y. and Yoshida N. (2011) Ultraviolet absorption cross sections of carbonyl sulfide isotopologues (OCS)-S-32, (OCS)-S-33, (OCS)-S-34 and (OCS)-C-13: isotopic fractionation in photolysis and atmospheric implications. *Atmos. Chem. Phys.* **11**, 10293–10303.

Hattori S., Schmidt J. A., Johnson M. S., Danielache S. O., Yamada A., Ueno Y. and Yoshida N. (2013) SO2 photoexcitation mechanism links mass-independent sulfur isotopic fractionation in cryospheric sulfate to climate impacting volcanism. *Proc. Natl. Acad. Sci. USA*.

Hebrard E., Dobrijevic M., Loison J. C., Bergeat A., Hickson K. M. and Caralp F. (2013) Photochemistry of C3Hp hydrocarbons in Titan's stratosphere revisited. *Astron. Astrophys.*, 552.

Holland H. D. (1984) *The Chemical Evolution of the Atmosphere and Oceans*. Princeton University Press, Princeton.

Holland H. D. (2009) Why the atmosphere became oxygenated: a proposal. *Geochim. Cosmochim. Acta* **73**, 5241–5255.

Johnston D. T. (2011) Multiple sulfur isotopes and the evolution of Earth's surface sulfur cycle. *Earth Sci. Rev.* **106**, 161–183.

Johnson J. E., Webb S. M., Thomas K., Ono S., Kirschvink J. L. and Fischer W. W. (2013) Manganese-oxidizing photosynthesis before the rise of cyanobacteria. *Proc. Natl. Acad. Sci. USA* **110**, 11238–11243.

Kasting J. F. (2013) What caused the rise of oxygen? *Chem. Geol.* **362**, 13–25.

Kasting J. F., Pavlov A. A. and Siefert J. L. (2001) A coupled ecosystem-climate model for predicting the methane concentration in the Archean atmosphere. *Orig. Life Evol. Biosph.* **31**, 271–285.

Kendall B., Reinhard C. T., Lyons T., Kaufman A. J., Poulton S. W. and Anbar A. D. (2010) Pervasive oxygenation along late Archaean ocean margins. *Nat. Geosci.* **3**, 647–652.

Kharecha P., Kasting J. F. and Siefert J. (2005) A coupled atmosphere–ecosystem model of the early Archean Earth. *Geobiology* **3**, 53–76.

Kopf S. and Ono S. (2012) Sulfur mass-independent fractionation in liquid phase chemistry: UV photolysis of phenacylphenylsulfone as a case study. *Geochim. Cosmochim. Acta* **85**, 160–169.

Kump L. R. and Barley M. E. (2007) Increased subaerial volcanism and the rise of atmospheric oxygen 2.5 billion years ago. *Nature* **448**, 1033–1036.

Kurzweil F., Claire M., Thomazo C., Peters M., Hannington M. and Strauss H. (2013) Atmospheric sulfur rearrangement 2.7 billion years ago: evidence for oxygenic photosynthesis. *Earth Planet. Sci. Lett.* **366**, 17–26.

Lin Y., Sim M. S. and Ono S. (2011) Multiple-sulfur isotope effects during photolysis of carbonyl sulfide. *Atmos. Chem. Phys.* **11**, 10283–10292.

Luz B., Barkan E., Bender M. L., Thiemens M. H. and Boering K. A. (1999) Triple-isotope composition of atmospheric oxygen as a tracer of biosphere productivity. *Nature* **400**, 547–550.

Lyons J. R. (2007) Mass-independent fractionation of sulfur isotopes by isotope-selective photodissociation of SO_2. *Geophys. Res. Lett.* **34**, 5.

Lyons J. R. (2008) An estimate of the equilibrium speciation of sulfur vapor over solid sulfur and implications for planetary atmospheres. *J. Sulfur Chem.* **29**, 269–279.

Lyons J. R. (2009) Atmospherically-derived mass-independent sulfur isotope signatures, and incorporation into sediments. *Chem. Geol.* **267**, 164–174.

Masterson A. L., Farquhar J. and Wing B. A. (2011) Sulfur mass-independent fractionation patterns in the broadband UV photolysis of sulfur dioxide: pressure and third body effects. *Earth Planet. Sci. Lett.* **306**, 253–260.

Maynard J. B., Sutton S. J., Rumble, III, D. and Bekker A. (2013) Mass-independently fractionated sulfur in Archean paleosols: a

large reservoir of negative Delta S-33 anomaly on the early Earth. *Chem. Geol.* **362**, 74–81.
McLoughlin N., Grosch E. G., Kilburn M. R. and Wacey D. (2012) Sulfur isotope evidence for a Paleoarchean subseafloor biosphere, Barberton, South Africa. *Geology* **40**, 1031–1034.
Michalski G., Bohlke J. K. and Thiemens M. (2004) Long term atmospheric deposition as the source of nitrate and other salts in the Atacama Desert, Chile: new evidence from mass-independent oxygen isotopic compositions. *Geochim. Cosmochim. Acta* **68**, 4023–4038.
Oduro H., Harms B., Sintim H. O., Kaufman A. J., Cody G. and Farquhar J. (2011) Evidence of magnetic isotope effects during thermochemical sulfate reduction. *Proc. Natl. Acad. Sci. USA* **108**, 17635–17638.
Ohmoto H., Watanabe Y., Ikemi H., Poulson S. R. and Taylor B. E. (2006) Sulphur isotope evidence for an oxic Archaean atmosphere. *Nature* **442**, 908–911.
Okabe H. (1978) *Photochemistry of Small Molecules*. John Wiley & Sons.
Olson J. M. (2006) Photosynthesis in the Archean Era. *Photosynth. Res.* **88**, 109–117.
Ono S., Eigenbrode J. L., Pavlov A. A., Kharecha P., Rumble, III, D., Kasting J. F. and Freeman K. H. (2003) New insights into Archean sulfur cycle from mass-independent sulfur isotope records from the Hamersley Basin, Australia. *Earth Planet. Sci. Lett.* **213**, 15–30.
Ono S., Beukes N. J., Rumble D. and Fogel M. L. (2006a) Early evolution of atmospheric oxygen from multiple-sulfur and carbon isotope records of the 2.9 Ga Mozaan Group of the Pongola Supergroup, Southern Africa. *S. Afr. J. Geol.* **109**, 97–108.
Ono S., Wing B., Johnston D., Farquhar J. and Rumble D. (2006b) Mass-dependent fractionation of quadruple stable sulfur isotope system as a new tracer of sulfur biogeochemical cycles. *Geochim. Cosmochim. Acta* **70**, 2238–2252.
Ono S. H., Beukes N. J. and Rumble D. (2009a) Origin of two distinct multiple-sulfur isotope compositions of pyrite in the 2.5 Ga Klein Naute Formation, Griqualand West Basin, South Africa. *Precambrian Res.* **169**, 48–57.
Ono S. H., Kaufman A. J., Farquhar J., Sumner D. Y. and Beukes N. J. (2009b) Lithofacies control on multiple-sulfur isotope records and Neoarchean sulfur cycles. *Precambrian Res.* **169**, 58–67.
Ono S., Whitehill A. R. and Lyons J. R. (2013) Contribution of isotopologue self-shielding to sulfur mass-independent fractionation during sulfur dioxide photolysis. *J. Geophys. Res. Atmos.* **118**, 2444–2454.
Pavlov A. A. and Kasting J. F. (2002) Mass-independent fractionation of sulfur isotopes in Archean sediments: strong evidence for an anoxic Archean atmosphere. *Astrobiology* **2**, 27–41.
Pavlov A. A., Kasting J. F. and Brown L. L. (2001) UV-shielding of NH_3 and O_2 by organic hazes in the Archean atmosphere. *J. Geophys. Res.* **106**, 1–23.
Pavlov A. A., Mills M. J. and Toon O. B. (2005) Mystery of the volcanic mass-independent sulfur isotope fractionation signature in the Antarctic ice core. *Geophys. Res. Lett.*, 32.
Petrash D. A., Gingras M. K., Lalonde S. V., Orange F., Pecoits E. and Konhauser K. O. (2012) Dynamic controls on accretion and lithification of modern gypsum-dominated thrombolites, Los Rogues, Venezuela. *Sed. Geol.* **245**, 29–47.
Philippot P., Van Zuilen M., Lepot K., Thomazo C., Farquhar J. and Van Kranendonk M. J. (2007) Early Archaean microorganisms preferred elemental sulfur, not sulfate. *Science* **317**, 1534–1537.
Philippot P., van Zuilen M. and Rollion-Bard C. (2012) Variations in atmospheric sulphur chemistry on early Earth linked to volcanic activity. *Nat. Geosci.* **5**, 668-U100.
Roerdink D. L., Mason P. R. D., Farquhar J. and Reimer T. (2012) Multiple sulfur isotopes in Paleoarchean barites identify an important role for microbial sulfate reduction in the early marine environment. *Earth Planet. Sci. Lett.* **331**, 177–186.
Roerdink D. L., Mason P. R. D., Whitehouse M. J. and Reimer T. (2013) High-resolution quadruple sulfur isotope analyses of 3.2 Ga pyrite from the Barberton Greenstone Belt in South Africa reveal distinct environmental controls on sulfide isotopic arrays. *Geochim. Cosmochim. Acta* **117**, 203–215.
Savarino J., Bekki S., Cole-Dai J. H. and Thiemens M. H. (2003) Evidence from sulfate mass independent oxygen isotopic compositions of dramatic changes in atmospheric oxidation following massive volcanic eruptions. *J. Geophys. Res. Atmos.* **108**.
Shen Y. N. and Buick R. (2004) The antiquity of microbial sulfate reduction. *Earth Sci. Rev.* **64**, 243–272.
Shen Y., Farquhar J., Masterson A., Kaufman A. J. and Buick R. (2009) Evaluating the role of microbial sulfate reduction in the early Archean using quadruple isotope systematics. *Earth Planet. Sci. Lett.* **279**, 383–391.
Stüeken E. E., Catling D. C. and Buick R. (2012) Contributions to late Archaean sulphur cycling by life on land. *Nat. Geosci.* **5**, 722–725.
Thiemens M. H. and Heidenreich J. E. (1983) The mass-independent fractionation of oxygen – a novel isotope effect and its possible cosmochemical implications. *Science* **219**, 1073–1075.
Thomazo C., Ader M., Farquhar J. and Philippot P. (2009) Methanotrophs regulated atmospheric sulfur isotope anomalies during the Mesoarchean (Tumbiana Formation, Western Australia). *Earth Planet. Sci. Lett.* **279**, 65–75.
Thomazo C., Nisbet E. G., Grassineau N. V., Peters M. and Strauss H. (2013) Multiple sulfur and carbon isotope composition of sediments from the Belingwe Greenstone Belt (Zimbabwe): a biogenic methane regulation on mass independent fractionation of sulfur during the Neoarchean? *Geochim. Cosmochim. Acta* **121**, 120–138.
Toon O. B., McKay C. P., Ackerman T. P. and Santhanam K. (1989) Rapid calculation of radiative heating rates and photodissociation rates in inhomogeneous multiple scattering atmospheres. *J. Geophys. Res.* **94**, 16287–16301.
Trainer M. G., Pavlov A. A., DeWitt H. L., Jimenez J. L., McKay C. P., Toon O. B. and Tolbert M. A. (2006) Organic haze on Titan and the early Earth. *Proc. Natl. Acad. Sci. USA* **103**, 18035–18042.
Ueno Y., Ono S., Rumble D. and Maruyama S. (2008) Quadruple sulfur isotope analysis of ca. 3.5 Ga Dresser Formation: new evidence for microbial sulfate reduction in the early Archean. *Geochim. Cosmochim. Acta* **72**, 5675–5691.
Ueno Y., Johnson M. S., Danielache S. O., Eskebjerg C., Pandey A. and Yoshida N. (2009) Geological sulfur isotopes indicate elevated OCS in the Archean atmosphere, solving faint young sun paradox. *Proc. Natl. Acad. Sci. USA* **106**, 14784–14789.
Watanabe Y., Farquhar J. and Ohmoto H. (2009) Anomalous fractionations of sulfur isotopes during thermochemical sulfate reduction. *Science* **324**, 370–373.
Whitehill A. R. and Ono S. (2012) Excitation band dependence of sulfur isotope mass-independent fractionation during photochemistry of sulfur dioxide using broadband light sources. *Geochim. Cosmochim. Acta* **94**, 238–253.
Whitehill A. R., Xie C., Hu X., Xie D., Guo H. and Ono S. (2013) Vibronic origin of sulfur mass-independent isotope effect in photoexcitation of SO_2 and the implications to the early earth's atmosphere. *Proc. Natl. Acad. Sci. USA*.

Wolf E. T. and Toon O. B. (2010) Fractal organic hazes provided an ultraviolet shield for early Earth. *Science* **328**, 1266–1268.

Yung Y. L. (1976) A numerical method for calculating the mean intensity in an inhomogeneous Rayleigh scattering atmosphere. *J. Quant. Spectrosc. Radiat. Transfer* **16**, 755–761.

Zahnle K. J., Claire M. W. and Catling D. C. (2006) The loss of mass-independent fractionation in sulfur due to a Paleoproterozoic collapse of atmospheric methane. *Geobiology* **4**, 271–283.

Zerkle A. L., Claire M., Domagal-Goldman S. D., Farquhar J. and Poulton S. W. (2012) A bistable organic-rich atmosphere on the Neoarchaean Earth. *Nat. Geosci.* **5**, 359–363.

Zmolek P., Xu X. P., Jackson T., Thiemens M. H. and Trogler W. C. (1999) Large mass independent sulfur isotope fractionations during the photopolymerization of (CS2)-C-12 and (CS2)-C-13. *J. Phys. Chem. A* **103**, 2477–2480.

Associate editor: Marc Norman